Microbiology (2005), **151**, 2053–2064 **DOI** 10.1099/mic.0.27899-0

ftsZ mutations affecting cell division frequency, placement and morphology in *Bacillus subtilis*

Andrea Feucht and Jeffery Errington

Sir William Dunn School of Pathology, University of Oxford, South Parks Road, Oxford OX1 3RE, UK

Correspondence
Jeffery Errington
jeff.errington@pathology.ox.ac.uk

Received 18 January 2005
Revised 8 March 2005
Accepted 10 March 2005

A key event in cytokinesis in bacteria is the assembly of the essential division protein FtsZ into ring-like structures at the nascent division site. FtsZ is the prokaryotic homologue of tubulin, and is found in nearly all bacteria. *In vitro*, FtsZ polymerizes in the presence of GTP to form higher-ordered polymers. FtsZ consists of two domains, with the GTP-binding site located in the N-terminal domain. The less-conserved C-terminal domain contains residues important for GTP hydrolysis, but its overall function is still unclear. This paper reports the development of a simple strategy to generate mutations in the essential division gene *ftsZ*. Nine novel and viable *ftsZ* mutants of *Bacillus subtilis* are described. Eight of the mutations would affect the C-terminus of FtsZ. The collection of mutants exhibits a range of morphological phenotypes, ranging from normal to highly filamentous cells; some produce minicells, or divide in a twisted configuration; one mutation has a temperature-sensitive effect specifically impairing sporulation. The sites of the amino acid changes generated by the mutations could be informative about FtsZ function and its protein–protein interactions.

INTRODUCTION

A fundamental problem in prokaryotes is the nature of the mechanism of cell division, which is tightly coupled to cell growth, chromosome replication and segregation. Thereby, the cell ensures that each daughter cell is of equal size, and inherits a complete genome. Cytokinesis in bacteria begins with the assembly of the essential GTPase FtsZ into a ring structure at the nascent division site (reviewed by Errington *et al.*, 2003; Romberg & Levin, 2003). FtsZ homologues can be found in nearly all bacteria, and have also been found in a number of eukaryotic organelles, e.g. mitochondria and chloroplasts (reviewed by Vaughan *et al.*, 2004). The crystal structure of FtsZ closely resembles that of eukaryotic α- and β-tubulin (Lowe & Amos, 1998; Nogales *et al.*, 1998). FtsZ consists of two domains, of which the GTP-binding interactions lie in its N-terminal domain (Lowe & Amos, 1998). The GTPase is split across two monomers, with the N-terminal domain of one monomer providing the GTP-binding site, and the C-terminal domain of the other nucleotide hydrolysis (Lowe & Amos, 1999; Scheffers *et al.*, 2002). Like tubulin, FtsZ undergoes GTP/GDP-dependent polymerization, forming protofilaments, sheets and mini-rings *in vitro* (Bramhill & Thompson, 1994; Erickson *et al.*, 1996; Mukherjee & Lutkenhaus, 1994, 1998; Yu & Margolin, 1997). The extreme C-terminus of FtsZ, which is not visible in the crystal structure, has been shown to be required for interaction with the essential division proteins FtsA and ZipA in *Escherichia coli* (Ma & Margolin, 1999; Mosyak *et al.*, 2000). In the rod-shaped bacterium *Bacillus subtilis*, six additional proteins, FtsA, FtsW, DivIB, DivIC, FtsL and PBP2B, have been implicated in cell division, and their localization to the division site is dependent on FtsZ (Beall & Lutkenhaus, 1992; Daniel & Errington, 2000; Daniel *et al.*, 2000; Feucht *et al.*, 2001; Katis *et al.*, 2000). Therefore, the FtsZ ring provides a cytoskeletal scaffold that recruits these other division proteins to form the cytokinetic machinery, and directs the ingrowth of the septum. FtsA, ZapA and the sporulation-specific protein SpoIIE have been shown to interact directly with FtsZ to stabilize FtsZ ring formation, but so far little is known about the residues that are involved in these interactions (Ben-Yehuda & Losick, 2002; Gueiros-Filho & Losick, 2002; Low *et al.*, 2004; Lucet *et al.*, 2000; Wang *et al.*, 1997).

On starvation, a developmental process called sporulation is initiated, and early in sporulation, the medial FtsZ ring disassembles and spirals out towards the cell poles, where it reassembles into a ring structure near both cell poles (Ben-Yehuda & Losick, 2002). The shift in position of the Z-ring depends both on an increase in FtsZ expression levels, and on the sporulation-specific SpoIIE protein. SpoIIE is an integral membrane protein that interacts directly with FtsZ (Lucet *et al.*, 2000), and it has been known for several years that polar FtsZ ring formation and asymmetric division are impaired in *spoIIE*-null mutants (Barak & Youngman, 1996; Feucht *et al.*, 1996; Khvorova *et al.*, 1998). Additionally,

Abbreviations: DAPI, 4′,6-diamidino-2-phenylindole; IFM, immunofluorescence microscopy.

SpoIIE plays a key role in σ^F activation (reviewed by Errington, 2003).

So far, three factors that act negatively on FtsZ ring formation have been described in *B. subtilis*: the Min system, the nucleoid and the Z-ring-associated protein EzrA. The Min system consists of three proteins, MinC, MinD and DivIVA, which prevent cell division near the cell pole (Marston & Errington, 1999). Recently, Wu & Errington (2004) identified a protein, Noc, that associates non-specifically with the nucleoid, and is required to inhibit cell division in its vicinity. EzrA is a membrane protein that interacts directly with FtsZ to prevent polymerization and aberrant FtsZ formation (Haeusser *et al.*, 2004).

The role of FtsZ in assembly and constriction of the division machinery is still not fully understood, and the above survey shows that there are a myriad of potential protein–protein interactions involving FtsZ, of which only a few have been characterized in any detail. The isolation of point mutations in *ftsZ* with subtle effects on phenotype might provide an important tool to analyse FtsZ function. Most previous genetic studies of *ftsZ* have focused on the isolation of mutants with severe division defects (Stricker & Erickson, 2003).

In this paper, we describe a new approach to the isolation of *ftsZ* mutants in *B. subtilis*, and describe nine new *ftsZ* mutants that are viable, and have mild, but potentially informative, phenotypes.

METHODS

Strains and plasmids. These are described in Table 1. Plasmid pSG1928 was constructed by cloning a 1158 bp DNA fragment containing the *B. subtilis ftsZ* gene without the ATG start codon into plasmid pSG1301. The DNA segment was amplified by PCR using 168 wild-type chromosomal DNA with primers 5′-GCTCTAGA-TTGGAGTTCGAAACAAACATA-3′ and 5′-CGGAATTCTTAGCC-GCGTTTATTACGG-3′, which introduced *Xba*I and *Eco*RI sites, respectively, and these were then used for cloning. The cloned *ftsZ* fragment was sequenced, and thereby several discrepancies from the published sequence were found (Beall *et al.*, 1988): codon 327 (CGT instead of CGC), codon 345 (GAG instead of GAC) and codon 346 (CCA instead of GCA). In several other independent PCR reactions using either 168 or SG38 wild-type chromosomal DNA as a template, we invariably found the same sequences as for the cloned construct. Site-directed mutagenesis (Stratagene) was used to introduce mutations into the *ftsZ* fragment of plasmid pSG1928. The following primers were used: (38-1fw) 5′-GTT-ATTAATGAAAATCCAAAAGATGAGATTGTGG-3′; (38-1rev) 5′-CCACAATCTCATCTTTTGGATTTTCATTAATAAC-3′; (38-2fw) 5′-GAGGAACCTCAGCGGCAGAACACAGTAAGC-3′; and (38-2rev) 5′-GCTTACTGTGTTCTGCCGCTGAGGTTCCTC-3′. Each mutant plasmid was sequenced before introduction into the *B. subtilis* chromosome. Also, the mutated *ftsZ* gene was sequenced from the chromosome of constructed strains to verify the *ftsZ* mutation. *ftsZ* mutations were crossed back into the parental strain by preparing and then transforming their chromosomal DNA into the parental strain, with selection for chloramphenicol resistance.

General methods. DNA manipulations and *E. coli* transformations were carried out using standard methods (Sambrook *et al.*, 1989). *B. subtilis* chromosomal DNA was prepared by a scaled-down method based on the one described by Errington (1984). *B. subtilis* cells were made competent for transformation with DNA using the method of Anagnostopoulos & Spizizen (1961), as modified by Jenkinson (1983). Nutrient agar (NA; Oxoid) was used as a solid medium, and PAB (Oxoid Antibiotic Medium no. 3) or hydrolysed casein medium (CH) as a liquid medium for growing *B. subtilis*. Chloramphenicol (5 μg ml^{-1}), tetracycline (10 μg ml^{-1}), erythromycin (1 μg ml^{-1}), lincomycin (25 μg ml^{-1}) and 0·01 % X-Gal were added as required. *E. coli* strains were grown in 2 × TY medium (Sambrook *et al.*, 1989) or on NA supplemented with ampicillin (100 μg ml^{-1}), as required.

Sporulation and β-galactosidase assay. Sporulation was induced by growth in CH, followed by resuspension in a starvation medium (SM) (Partridge & Errington, 1993; Sterlini & Mandelstam, 1969). Time zero (t_0) was defined as the point at which the cells were resuspended in the SM. Measurement of septum formation and sporulation frequency was performed as described previously (Feucht *et al.*, 2002).

β-Galactosidase activity was assayed using a method described by Errington & Mandelstam (1986). One unit of β-galactosidase catalyses the production of 1 nmol 4-methylumbelliferone min^{-1}.

Western blot analysis. Strains were inoculated in PAB, and grown for 3 h at 37 °C. Culture samples (0·5 ml) were taken, boiled (5 min), and equal amounts of proteins were loaded and separated by 10 % SDS-PAGE. The amount of protein was determined by a Bio-Rad assay. The proteins were then transferred to Hybond-C membranes (Amersham), and subjected to immunoblotting with polyclonal anti-FtsZ antibodies, which were used at a dilution 1 : 2000. Alkaline-phosphatase-conjugated antibodies were used as secondary antibodies, and blots were developed by exposure to ECL substrate (Amersham).

Microscopy. For phase-contrast and fluorescence visualization, samples of live cells were examined either on glass slides pre-treated with polysine, or on a thin film of 1·2 % agarose. Membranes were stained with FM5-95 (final concentration 90 μg ml^{-1}; Molecular Probes) by adding the dye at least 20 min prior to microscopy examination. Nucleoids were stained by adding 3 μl 4′,6-diamidino-2-phenylindole (DAPI; 1 μg ml^{-1} in 50 %, v/v, glycerol; Sigma) to 9 μl cells for 1 min before viewing. Images were acquired using a Sony CoolSnap HQ cooled CCD camera (Roper Scientific) attached to an Axiovert 135TV inverted microscope (Zeiss) and METAMORPH version 4.6 software (Universal Imaging Corporation). Rabbit polyclonal anti-FtsZ antibodies were used for immunofluorescence microscopy (IFM) at a dilution of 1 : 400. Fixation, permeabilization and immunofluorescence staining of cells were performed as described previously (Lewis & Errington, 1996; Pogliano *et al.*, 1995; Resnekov *et al.*, 1996), except that the glutaraldehyde concentration was reduced to 0·005 %.

RESULTS

Isolation of non-lethal *ftsZ* mutations

A plasmid carrying the *ftsZ* gene, but lacking the first ATG codon, was randomly mutagenized by propagation in the *E. coli* mutator strain XL1-Red (Stratagene). The mutagenized plasmid library was transformed into several different *B. subtilis* strains, with selection for plasmid integration via single crossover into the host chromosome on the basis of chloramphenicol resistance. The resultant clones contained a mutated, but full-length, copy of *ftsZ*, under its natural

Table 1. Strains and plasmids

Strain/plasmid	Relevant genotype†	Construction‡, source or reference
B. subtilis		
BFS1038*	*trpC2 ezrA*::pMUTIN2.mcs (*ermC*)	Laboratory stock
FG356	*zapA–yshB*Δ::*tet amyE*::P_{xyl}-*zapA* (*cat*) *thrC*::P_{spac}-*yshB* (*erm*)	Gueiros-Filho & Losick (2002)
SG38	*trpC2 amyE*	Errington & Mandelstam (1986)
168	*trpC2*	Laboratory stock
279.1	*metC3 tal-1 ftsA279*	Young (1976)
1272	*trpC2* Δ(*yoaV*::*spoIIQ′–′lacZ ermC*)	L. J. Wu, University of Oxford (unpublished)
1356	*trpC2 zapA–yshB*Δ::*tet*	FG356→168 (Tc)
1357	As 1272 Ω[*ftsZ*::pSG1928 *ftsZ3* (V260A) *cat*]	pSG1928§→1272 (Cm)
1358	As 1272 Ω[*ftsZ*::pSG1928 *ftsZ4* (A285T) *cat*]	pSG1928§→1272 (Cm)
1359	As 1272 Ω[*ftsZ*::pSG1928 *ftsZ6* (E300K) *cat*]	pSG1928§→1272 (Cm)
1360	As 1272 Ω[*ftsZ*::pSG1928 *ftsZ11* (S271R) *cat*]	pSG1928§→1272 (Cm)
1361	As 1272 Ω[*ftsZ*::pSG1928 *ftsZ24* (I245F) *cat*]	pSG1928§→1272 (Cm)
1362	As 1901 Ω[*ftsZ*::pSG1928 *ftsZ20* (V38A) *cat*]	pSG1928§→1901 (Cm)
1363	As 1901 Ω[*ftsZ*::pSG1928 *ftsZ5* (D174N) *cat*]	pSG1928§→1901 (Cm)
1364	As 1901 Ω[*ftsZ*::pSG1928 *ftsZ38* (L302P, Q353R) *cat*]	pSG1928§→1901 (Cm)
1365	As 2770 Ω[*ftsZ*::pSG1928 *ftsZ8* (S219L) *cat*]	pSG1928§→2770 (Cm)
1366	As 1272 Ω[*ftsZ*::pSG1928 *ftsZ20* (V38A) *cat*]	1362→1272 (Cm)
1367	As 1272 Ω[*ftsZ*::pSG1928 *ftsZ5* (D174N) *cat*]	1363→1272 (Cm)
1368	As 1272 Ω[*ftsZ*::pSG1928 *ftsZ38* (L302P, Q353R) *cat*]	1364→1272 (Cm)
1369	As 1272 Ω[*ftsZ*::pSG1928 *ftsZ8* (S219L) *cat*]	1365→1272 (Cm)
1370	As 168 Ω[*ftsZ*::pSG1928 *ftsZ38-1*(L302P) *cat*]	pSG1929→1272 (Cm)
1371	As 168 Ω[*ftsZ*::pSG1928 *ftsZ38-2* (Q353R) *cat*]	pSG1930→1272 (Cm)
1372	As 1272 Ω(*ftsZ*::pSG1928 *cat*)	pSG1928→1272 (Cm)
1901	*trpC2 amyE* Ω(*minD*::*ermC*)	Marston *et al.* (1998)
2023	*trpC2 amyE noc*::*ermC*	Sievers *et al.* (2002)
2770	*trpC2* Δ*minCD*::*ermC*	A. Leung, University of Oxford (unpublished)
E. coli		
MC1061	F$^-$ *hsdR mcrB araD139* Δ(*araABC–leu*)*7679 galU galK* Δ(*lac*)*X74 rpsL thi*	Meissner *et al.* (1987)
XL1-Red	*endA1 gyrA96 thi-1 hsdR17 supE44 relA1 lac mutD5 mutS mutT* Tn*10* (Tet)	Stratagene
Plasmids		
pSG1301	*bla cat*	Stevens *et al.* (1992)
pSG1928	*bla cat ftsZ*(*4-1146*)	This study
pSG1929	*bla cat ftsZ38-1*(L302P)	pSG1928 containing the *ftsZ38-1* (L302P) mutation
pSG1930	*bla cat ftsZ38-2*(Q353R)	pSG1928 containing the *ftsZ38-2* (Q353R) mutation

*Strain generated by the *B. subtilis* genome function project.

†Numbers in parentheses after *ftsZ* refer to the first and last nucleotides of the *ftsZ* coding sequence.

‡For DNA transformations, the source of the DNA is shown, followed by an arrow, then the recipient strain, with the antibiotic selection in parentheses.

§The plasmid was mutagenized.

transcriptional control, followed by the integrated plasmid and a second (inactive) copy of *ftsZ* that lacked promoter, ribosome-binding site and start codon sequences. The library of mutant *ftsZ* alleles was screened in two ways. The first screen was based on use of a strain (1272) bearing a σ^F-dependent *spoIIQ–lacZ* reporter gene. σ^F activation during sporulation is dependent on formation of the asymmetric division septum (Feucht *et al.*, 1999; King *et al.*, 1999). This reporter is also inhibited by perturbations in vegetative cell length, which affect polar septation during

sporulation indirectly. Transformants of this strain were grown at 37 °C, and screened for decreased or increased σ^F activation on the basis of β-galactosidase activity on plates containing X-Gal. Of approximately 30 000 transformants screened, five mutants were obtained that formed colonies which were either darker (mutant *ftsZ24*) or paler blue (mutants *ftsZ3*, *ftsZ4*, *ftsZ6* and *ftsZ11*), suggesting an altered activation of σ^F compared with the parental strain. The colour changes in strains carrying the *ftsZ3* or *ftsZ4* mutation were slight. All five mutations were crossed back into the parental strain 1272. Segregation of darker and lighter blue colonies confirmed that the mutations lay within the *ftsZ* locus.

In parallel, the mutated plasmid library was also transformed into host strains 1901 and 2770 containing deletions of *minD* and *minCD*, respectively. Both strains are slightly impaired in sporulation (Levin *et al.*, 1998; Thomaides *et al.*, 2001). Transformants were grown at 37 °C, and screened for altered sporulation frequency on the basis of colony appearance. Around 4500 and 9000 transformants were screened, yielding three mutations (*ftsZ5*, *ftsZ20* and *ftsZ38*) from the *minD* mutant, and one (*ftsZ8*) from the *minCD* mutant. All of the mutants appeared to be further impaired in sporulation than the parental strain on NA. The mutations were crossed into the *minCD*$^+$ strain 1272. Segregation of mutations *ftsZ5*, *ftsZ20* and *ftsZ38* into colonies with normal and reduced sporulation efficiency showed that these mutations also had an effect in the wild-type background, and lay within the *ftsZ* locus. Mutation *ftsZ8*, which produced only a slight sporulation defect in 2770, did not have a detectable phenotype in the wild-type background. Therefore the presence of the mutation was confirmed by sequencing the *ftsZ* gene of four transformants.

DNA sequencing (Table 2) revealed that only one of the new *ftsZ* alleles, *ftsZ20*, would produce a substitution (V38A) in the N-terminal domain of the protein. Allele *ftsZ5* (D174N) would affect the beginning of the core helix H7 that connects the N- and C-terminal domains of FtsZ. Six of the other seven alleles had mutations that would affect residues in the less-characterized C-terminal domain of FtsZ. The exception, *ftsZ38*, had two mutations: L302P, which lay close to the *ftsZ6* mutation, and Q353R, which lay in the extreme C-terminus, for which no structural data are available. The substitution V38A (*ftsZ20*) is in an amino acid position that is highly conserved between other organisms for which genome sequences are available (Vaughan *et al.*, 2004). The changes I245F (*ftsZ24*), V260A (*ftsZ3*), E300K (*ftsZ6*), L302P (*ftsZ38*) are in less-conserved residues, whereas D174N (*ftsZ5*), S219L (*ftsZ8*), S271R (*ftsZ11*), A285T (*ftsZ4*) and Q353R (*ftsZ38*) are not conserved (Vaughan *et al.*, 2004).

Morphology of the *ftsZ* mutant strains

To examine the morphological phenotype of the mutants in more detail, cultures of the wild-type and mutant strains were grown in PAB, and exponentially growing cells were analysed by microscopy (Fig. 1). At this point, each of the mutations was examined in a *min*$^+$ background, independent of the background in which it was isolated. The wild-type strain (1272) is illustrated in Fig. 1(A). Cells producing FtsZS219L (*ftsZ8*; Fig. 1B, C) had a mild phenotype manifested only in the presence of a small percentage (<1 %) of minicells (arrow in Fig. 1B). In the *minCD* strain background that the mutation was originally isolated from, it formed abnormally long cells (Fig. 1D), which probably accounts for the reduction in sporulation frequency that led to its isolation.

Several mutant proteins [FtsZI245F (*ftsZ24*), FtsZL302P-Q353R (*ftsZ38*), FtsZV260A (*ftsZ3*) and FtsZA285T (*ftsZ4*)]

Table 2. Phenotypic effects of *ftsZ* mutants in the wild-type

Mutation	Derivation*	Amino acid change	FtsZ localization pattern in wild-type background	Morphological phenotype in wild-type background†
ftsZ3	*IIQ*↓	V260A	Normal, extra protein at cell poles	Spo$^+$; ~10 % minicells
ftsZ4	*IIQ*↓	A285T	Normal, extra protein at cell poles	Spo$^+$; ~10 % minicells
ftsZ6	*IIQ*↓ ↓	E300K	Broad diffuse bands, aberrant structures	Spo$^-$; normal and filamentous cells; twisted divisions
ftsZ11	*IIQ*↓ ↓	S271R	Long helices	Spo$^-$; normal and filamentous cells
ftsZ24	*IIQ*↑	I245F	Normal	Spo$^+$; ~5 % minicells
ftsZ20	*minD*	V38A	Helices	Spo$^{+/-}$; twisted divisions
ftsZ5	*minD*	D174N	Normal, helices, aberrant structures	Spo$^{+/-}$; normal and slightly filamentous cells
ftsZ38	*minD*	L302P (Q353R)	Normal, short helices	Spo^{ts}; ~5 % minicells
ftsZ8	*minCD*	S219L	Normal, some helices, extra protein at cell poles	Spo$^+$; <1 % minicells

*Mutations were identified in a *minD* background, a *minCD* background, or a wild-type background, as a colony showing increased (*IIQ*↑), decreased (*IIQ*↓) or severely decreased (*IIQ*↓ ↓) expression of a *spoIIQ–lacZ* fusion.

†Spo$^+$, sporulation proficient; Spo$^{+/-}$, weak sporulation defect; Spo$^-$, strong sporulation defect; as judged by colony appearance on NA incubated at 37 °C.

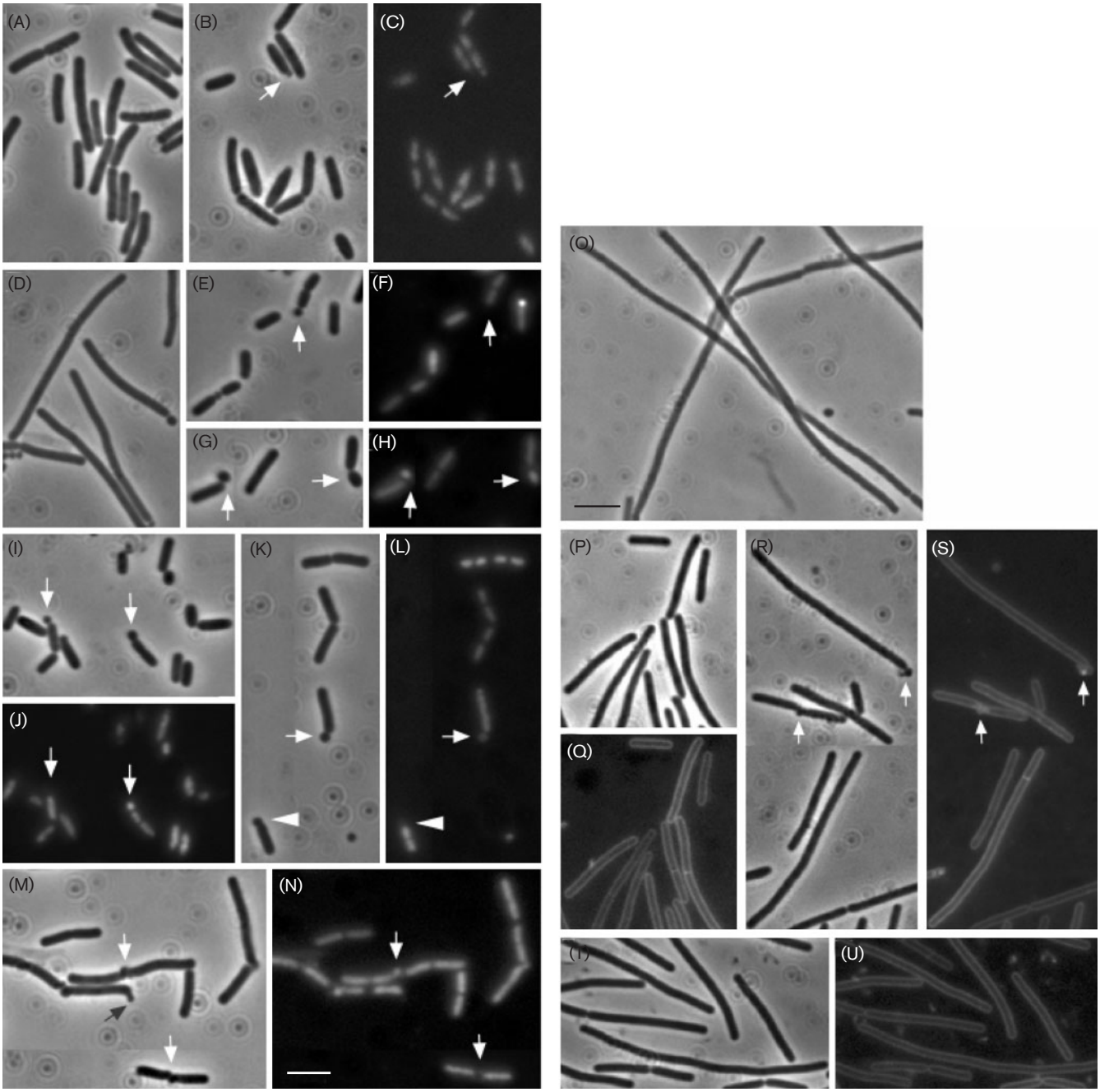

Fig. 1. Morphological phenotype of the mutant *ftsZ* strains. Exponentially growing cells were stained with DAPI or FM5-95 to visualize the nucleoids or membranes, respectively. Phase-contrast (A, B, D, E, G, I, K, M, O, P, R and T) and fluorescence micrographs stained with DAPI (C, F, H, J, L and N) or FM5-95 (Q, S and U) of the same field of cells are shown. (A) Strain 1272 (wild-type), (B, C) strain 1369 (*ftsZ8*; FtsZS219L), (D) strain 1365 (Δ*minCD*, *ftsZ8*; FtsZS219L), (E, F) strain 1361 (*ftsZ24*; FtsZI245F), (G, H) strain 1368 (*ftsZ38*; FtsZL302P-Q353R), (I, J) strain 1357 (*ftsZ3*; FtsZV260A), (K, L) strain 1358 (*ftsZ4*; FtsZA285T), (M, N) strain 1366 (*ftsZ20*; FtsZV38A), (O) strain 1363 (*minD*, *ftsZ5*; FtsZD174N), (P, Q) strain 1367 (*ftsZ5*; FtsZD174N), (R, S) strain 1359 (*ftsZ6*; FtsZE300K), and (T, U) strain 1360 (*ftsZ11*; FtsZS271R). Scale bars, 5 μm.

caused the formation of significant numbers of minicells. As seen in Fig. 1(E) and (F), cells producing FtsZI245F protein (*ftsZ24*) looked slightly shorter than those of the wild-type, and up to about 5 % of the cells formed minicells (example arrowed). The majority of minicells were DNA free, but occasionally they contained DNA (data not shown). The FtsZL302P-Q353R protein (*ftsZ38*) also caused formation of ~5 % minicells, but in this case, unusually, the majority

of them contained DNA (Fig. 1G, H). Otherwise, the cell length was similar to that of the wild-type strain. The *ftsZ38* mutation was isolated in a *minD*$^-$ background, and originally large numbers of minicells were formed (data not shown). However, the mutation seemed to be unstable in the 1901 strain background, and derivatives showing improved growth developed within the colonies after a few days of growth on NA containing chloramphenicol. Cells producing FtsZV260A protein (*ftsZ3*) grew normally and produced ~10 % minicells, of which about half contained DNA (arrows in Fig. 1I, J). Production of the FtsZA285T protein (*ftsZ4*) generated cells with a similar cell-length distribution to that of the wild-type, though again ~10 % minicells were produced (Fig. 1K, L). For this mutant, the vast majority of the minicells contained no DNA [minicells with (arrow) and without (arrowhead) DNA are labelled].

Cells producing FtsZV38A protein (*ftsZ20*) had a slightly increased cell length (Fig. 1M, N). Around 15 % of sister cells appeared to divide in a twisted manner to produce a 'seagull' morphology (white arrows). Twisted divisions appeared to occur in both shorter and longer cells. Some of the twisted divisions trapped DNA in the septum (upper white arrow). Many cells had a misshaped pole with a pointed tip or a tilted minicell-like appendage (black arrow).

As shown in Fig. 1(O), the *ftsZ5* mutant (FtsZD174N), when first isolated in the *minD* background, formed long filaments. The phenotype was less severe in the wild-type background, and the cells were only slightly longer, on average, than the wild-type (Fig. 1P). Staining the membranes of the cells with the dye FM5-95 showed that some of the longer cells occasionally formed a septum (Fig. 1Q). Perhaps because of the impairment in division, *ftsZ5* mutant colonies appeared to be unstable in both *minD* and wild-type backgrounds when propagated on NA (with or without chloramphenicol selection).

Exponentially growing cells producing FtsZE300K (*ftsZ6*; Fig. 1R, S) and FtsZS271R (*ftsZ11*; Fig. 1T, U) mutant proteins formed a mixture of short wild-type-like cells and long filaments with few division septa (as seen by staining the membranes with FM9-95; Fig. 1S, U). In addition, production of FtsZE300K (*ftsZ6*) protein generated in some cells twisted divisions, either within or near the end of the cell filament, again forming tilted minicell-like appendages (arrows). This mutant also appeared to be unstable on NA, whereas the *ftsZ11* mutant strain was stable.

As some of the *ftsZ* mutant strains were unstable, all cultures were propagated in liquid PAB medium for minimal periods of time. As a further check on the reproducibility of the phenotypes, the mutants were also examined directly from NA, and also immediately after growth on the primary transformation plates, yielding similar findings (data not shown).

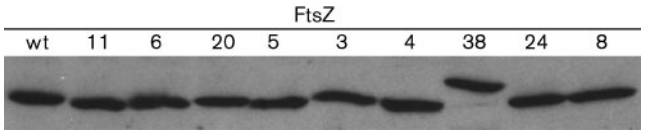

Fig. 2. Effects of the *ftsZ* mutations on protein stability. Whole-cell extracts of exponentially growing strains 1272 (wild-type, wt), 1360 (*ftsZ11*; FtsZS271R), 1359 (*ftsZ6*; FtsZE300K), 1366 (*ftsZ20*; FtsZV38A), 1367 (*ftsZ5*; FtsZD174N), 1357 (*ftsZ3*; FtsZV260A), 1358 (*ftsZ4*; FtsZA285T), 1368 (*ftsZ38*; FtsZL302P-Q353R), 1361 (*ftsZ24*; FtsZI245F) and 1369 (*ftsZ8*; FtsZS219L) were analysed by Western blot for FtsZ mutant protein levels using polyclonal anti-FtsZ antibodies.

It has been shown that lowering or increasing FtsZ expression levels causes filamentation or an increase in minicell formation, respectively (Palacios *et al.*, 1996; Ward & Lutkenhaus, 1985; Weart & Levin, 2003). Therefore, FtsZ protein levels in the various mutants were examined by Western blotting (Fig. 2). All of the mutants appeared to produce normal levels of FtsZ. Suprisingly, the FtsZL302P-Q353R protein (*ftsZ38*) ran at a higher molecular mass position, suggesting that the tertiary structure of this mutant protein might be altered or more resistant to SDS treatment. Sequencing of the *ftsZ38* gene from the chromosome verified the absence of any duplicated sequences.

FtsZ ring formation in the mutant *ftsZ* strains

To determine the effect of the mutations on FtsZ ring formation, we performed IFM on exponentially growing cells, using polyclonal anti-FtsZ antibodies. All mutations were analysed in the *minCD*$^+$ strain background (strain 1272). As shown in Fig. 3(A) and (B), FtsZ ring formation in cells producing FtsZI245F protein (*ftsZ24*) was indistinguishable from that of the wild-type strain, in which single bright transverse bands of fluorescence were evident near the midpoints of each cell. The majority of the FtsZI245F (*ftsZ24*) bands were correctly localized at mid-cell, either between separated sister nucleoids, or over bilobed-shaped nucleoids (the bilobed nucleoids have most likely terminated DNA replication, but not segregation; Sharpe *et al.*, 1998) (Fig. 3B, C). A few FtsZI245F (*ftsZ24*) bands localized close

Fig. 3. FtsZ structures in the *ftsZ* mutant strains. FtsZ was visualized in exponentially growing cells of strains (A) 1272 (wild-type), (B, C) 1361 (*ftsZ24*; FtsZI245F), (D, E) 1357 (*ftsZ3*; FtsZV260A), (F, G) 1358 (*ftsZ4*; FtsZA285T), (H, I) 1368 (*ftsZ38*; FtsZL302P-Q353R), (J, K) 1369 (*ftsZ8*; FtsZS219L), (L, M) 1366 (*ftsZ20*; FtsZV38A), (N, O) 1367 (*ftsZ5*; FtsZD174N), (P, Q) 1360 (*ftsZ11*; FtsZS271R), and (R, S) 1359 (*ftsZ6*; FtsZE300K), by IFM. Cells were immunostained with polyclonal anti-FtsZ antibodies (A, B, D, F, H, J, L, N, P and R), and stained for DNA with DAPI (C, E, G, I, K, M, O, Q and S). Scale bar, 5 μm.

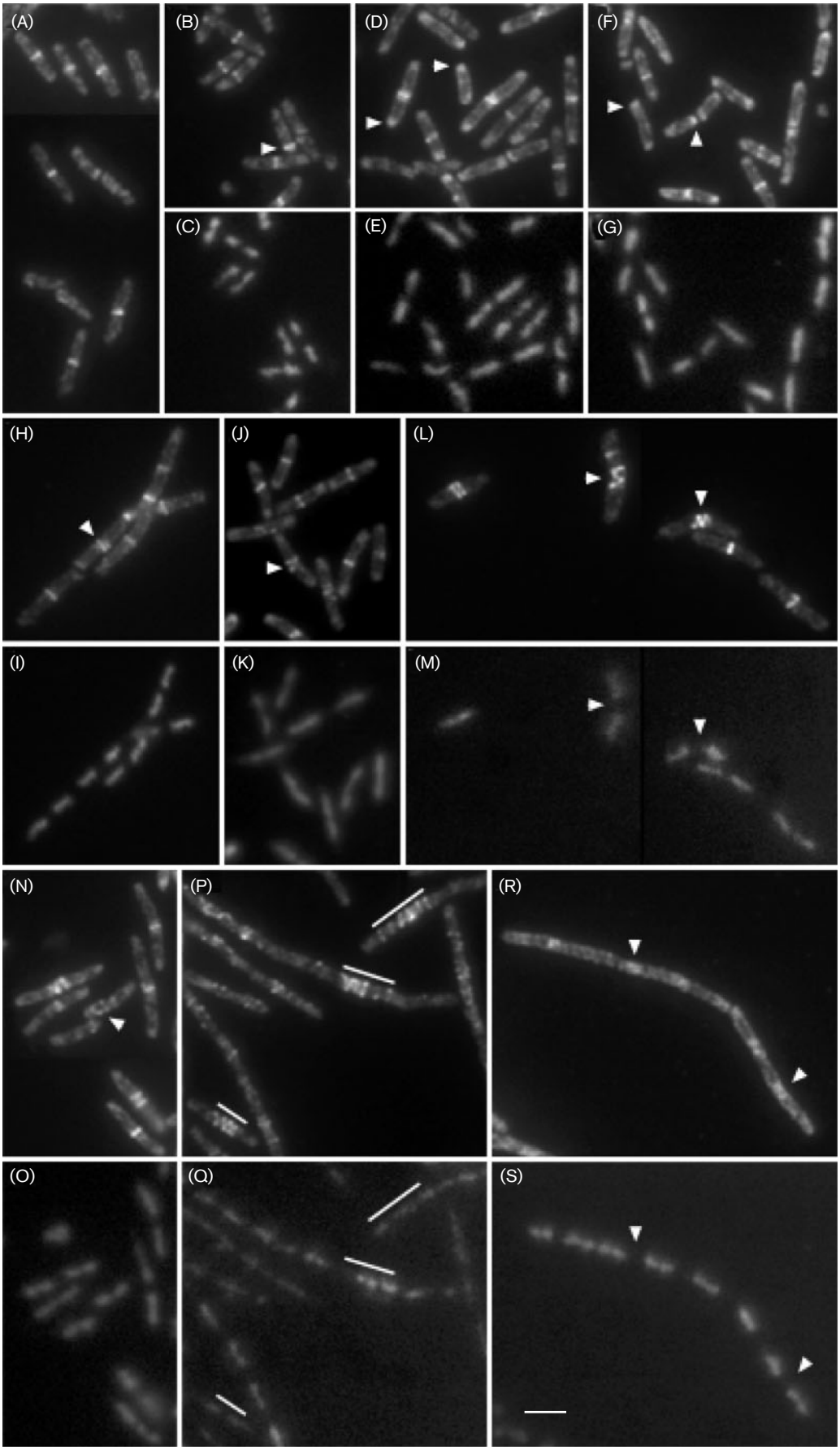
(A)
(B)
(D)
(F)
(C)
(E)
(G)
(H)
(J)
(L)
(I)
(K)
(M)
(N)
(P)
(R)
(O)
(Q)
(S)

to one pole of the cell (arrowhead), probably resulting in minicell formation.

The FtsZV260A (*ftsZ3*) and FtsZA285T (*ftsZ4*) proteins formed FtsZ rings similar to the wild-type, but, in addition, mutant cells frequently exhibited a strong fluorescent signal at the poles of the cell (Fig. 3D, F). This suggests that some FtsZ is retained there after septation, or that the mutant proteins are resistant to the normal action of the Min system in preventing FtsZ polymerization close to the poles.

A number of mutant proteins [FtsZL302P-Q353R (*ftsZ38*), FtsZS219L (*ftsZ8*) and FtsZV38A (*ftsZ20*)] formed helical FtsZ structures with one to two turns at mid-cell, in addition to normal FtsZ bands. The FtsZL302P-Q353R protein (*ftsZ38*) generated the weakest phenotype, with few helical FtsZ structures (Fig. 3H). The FtsZS219L protein (*ftsZ8*) formed helical structures in many cells, but they also usually had abnormal amounts of FtsZ at the poles (Fig. 3J). Interestingly, the gross morphology of this strain was nearly indistinguishable from that of the wild-type strain (apart from a few minicells), suggesting that the helical FtsZ structures at mid-cell eventually generate near-normal cell divisions. Production of the FtsZV38A protein (*ftsZ20*) caused the most severe defect, with most cells exhibiting helical FtsZ structures or double FtsZ bands (Fig. 3L), which also appeared to be helical structures when the focal plane was varied (not shown). Again, the near-normal length of the cells of this mutant supports the notion that the helical FtsZ rings usually lead to division. However, in this case the topology of division reflected the shape of the FtsZ structures, and many of the cells formed abnormal, twisted septa (see above).

The FtsZD174N protein (*ftsZ5*) formed a range of abnormal structures and accumulations of FtsZ (Fig. 3N). As cultures of this mutant included normal but also longer cells, some of the FtsZ structures are presumably non-functional.

Elongated helical FtsZ structures were particularly evident in mutant cells producing FtsZS271R (*ftsZ11*) mutant protein. The helices often overlapped the area occupied by the DNA (white bars in Fig. 3P, Q). A similar FtsZ localization pattern has been observed in cells with a disruption of the *noc* gene, which is required for nucleoid occlusion in *B. subtilis* (Wu & Errington, 2004).

FtsZE300K protein (*ftsZ6*) formed diffuse broad FtsZ structures, but in contrast to FtsZS271R (*ftsZ11*), these structures tended to be located between nucleoids (arrowheads in Fig. 3R, S). Most of the FtsZE300K (*ftsZ6*) structures are probably non-functional, as the strain forms elongated filaments, with only occasional cells of normal length.

Effects of the *ftsZ* mutations in various division-mutant backgrounds

The range of phenotypes exhibited by the collection of *ftsZ* mutants suggested that they might be affected in different aspects of FtsZ function, or interactions with other components of the division machinery. We reasoned that we might get more information by combining the *ftsZ* mutations with mutations in other division genes. Therefore, we attempted to introduce each of the new *ftsZ* mutations into strains bearing mutations in various division genes (*ezrA*, *ftsA279*, *minC*, *minD*, *noc* and *zapA*), none of which seriously affects growth under normal conditions, and look for additional effects on the phenotype.

Most of the *ftsZ* mutations (*ftsZ3*, *ftsZ4*, *ftsZ8*, *ftsZ11*, *ftsZ20*, *ftsZ24* and *ftsZ38*) had either only a weak or no additional phenotype when combined with any of the division mutations tested (data not shown). Two mutations, *ftsZ5* and *ftsZ6* (producing FtsZD174N and FtsZE300K, respectively), had lethal or near-lethal effects in most or all of the mutant backgrounds. The *ftsZ6* mutation had the most severe effect, and double-mutant progeny were recovered at greatly reduced frequency in combination with mutations in *ezrA*, *minD*, *minC* and *ftsA279*. The mutation was viable in combination with *zapA* or *noc* mutation, but the colonies were small. Therefore, production of FtsZE300K (*ftsZ6*) mutant protein makes cells sensitive to a range of perturbations of the division machinery that are normally well tolerated. FtsZD174N (*ftsZ5*) mutant protein caused a similar, but less severe, effect. The *ftsZ5* double mutants were generally viable, but the cells grew into long filaments, and sporulation was abolished. Absence of EzrA had the strongest effect, and double mutants could not be recovered at all.

Mutations *ftsZ24* and *ftsZ38* affect sporulation

Next we examined whether any of the *ftsZ* mutations that had approximately normal cell length, and produced FtsZ rings similar to those of the wild-type, had an effect on asymmetric cell division during sporulation, as measured by activation of the sporulation-specific σ-factor, σ^F (Feucht *et al.*, 1999; King *et al.*, 1999). Liquid cultures of various mutant strains were induced to sporulate, and β-galactosidase activity was measured from a *lacZ* fusion to the σ^F-dependent reporter gene *spoIIQ*. The *ftsZ3* and *ftsZ4* mutant strains (producing FtsZV260A and FtsZA285T, respectively) had a similar level of σ^F activity as an isogenic *ftsZ*$^+$ strain (data not shown). As shown in Fig. 4(A), an *ftsZ24* mutant (producing FtsZI245F) exhibited slightly higher β-galactosidase activity than the wild-type. In contrast, the *ftsZ38* mutant strain (producing FtsZL302P-Q353R) showed a drastically reduced β-galactosidase activity. These data were in good agreement with the darker and paler colour development seen on X-Gal plates by the *ftsZ24* and *ftsZ38* mutant strains, respectively. Interestingly, around 60 % of cells of strain 1368 (*ftsZ38*) appeared to have reached or gone beyond the stage of asymmetric septum completion 120 min after induction of sporulation (as judged by the formation of condensed prespore nucleoids; 64 % in the equivalent *ftsZ*$^+$ strain), suggesting that the reduced activation of σ^F is not due to a block in formation of the asymmetric septum. To determine which of the two

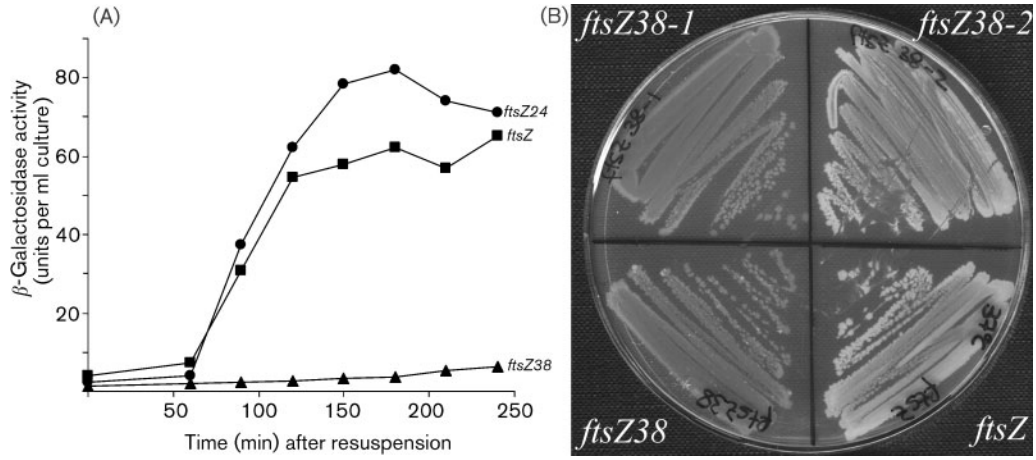

Fig. 4. Effects of the *ftsZ24* and *ftsZ38* mutations on sporulation. (A) Strains 1272 (wt), 1361 (*ftsZ24*; FtsZI245F) and 1368 (*ftsZ38*; FtsZL302P-Q353R) were induced to sporulate at 37 °C, and assayed at intervals for β-galactosidase activity produced from the σ^F-dependent *spoIIQ–lacZ* reporter gene. (B) Colony appearance after 2 days growth on NA containing chloramphenicol at 37 °C. The streaked-out strains are 1368 (*ftsZ38*; FtsZL302P-Q353R), 1370 (*ftsZ38-1*; FtsZL302P), 1371 (*ftsZ38-2*; FtsZQ353R) and 1372 (*ftsZ*).

substitutions in the original *ftsZ38* mutant was responsible for the impairment of sporulation, each mutation was reconstructed in the vector plasmid (pSG1928) using site-directed mutagenesis, and the mutations were introduced separately into strain 1272. Fig. 4(B) shows that the strain containing the mutation generating the Q353R (*ftsZ38-2*) substitution sporulated like the wild-type on plates grown at 37 °C, whereas the L302P (*ftsZ38-1*) substitution produced a defect in sporulation like that of the original double mutant. During the course of this work, we also observed that the *ftsZ38* mutant strain was temperature sensitive. Colonies grown at room temperature were indistinguishable for sporulation from the wild-type, whereas a defect in sporulation was detected when the strain was grown at 37 or 48 °C (Fig. 4B and data not shown). Preliminary results showed that the mean length of vegetative cells was not affected at higher growth temperatures, suggesting that the FtsZL302P-Q353R protein (*ftsZ38*) is specifically affected in sporulation (Fig. 1G, H and data not shown).

DISCUSSION

An important contribution of the present study is the development of a simple strategy to generate and analyse mutations in the essential division gene *ftsZ in vivo*. The N-terminal domain of FtsZ contains the GTP-binding site, and is involved in monomer–monomer interactions within a single protofilament (Lowe & Amos, 1998, 1999). In contrast, the C-terminal domain of FtsZ is far less conserved, and little is known about its function, except that it often seems to be the site for interaction with other proteins. Interestingly, eight out of the nine mutations described in this study would affect the C-terminus of FtsZ. All of the amino acid substitutions appear to localize in loops, or close to the beginning or end of a helix or sheet structure (Fig. 5), supporting the idea that the C-terminal fold of FtsZ is conserved, and that mutations affecting secondary structural elements are probably lethal, and therefore would not be picked up by this screening approach. All FtsZ mutant proteins, except FtsZS219L (*ftsZ8*), caused a morphological phenotype in the wild-type strain background, ranging from filaments, to minicells with and without DNA, to twisted cells (Fig. 1), suggesting that the C-terminal domain of FtsZ is important for topological features of cell division, particularly the location and orientation of FtsZ assembly.

Our data suggest that two of the mutant proteins, FtsZD174N (*ftsZ5*) and FtsZE300K (*ftsZ6*), might be affected in their ability to assemble, as both mutants grew into normal and filamentous cells, demonstrating that some of the aberrant FtsZ structures seen by IFM are nonfunctional (Figs 1 and 3). Additionally, combining these *ftsZ* mutations with mutations in other division genes had lethal or near-lethal effects, suggesting that both mutants require the action of accessory proteins for cell division, perhaps to stabilize FtsZ polymers, to disassemble aberrant structures, and/or to replenish the pool of soluble mutant FtsZ protein. Modelling the structure of the *B. subtilis* FtsZ (Fig. 5) using the solved protein structure of *Methanococcus jannaschii* FtsZ1 (Lowe & Amos, 1998; D. Brown, personal communication) suggests that the *ftsZ5* and *ftsZ6* mutations lie close together on one surface of the protein, consistent with these mutations having similar effects on the assembly of FtsZ polymers.

Bi & Lutkenhaus (1992) described the isolation of a temperature-sensitive *ftsZ26* mutant in *E. coli* that forms FtsZ spirals, and leads to the formation of spirally

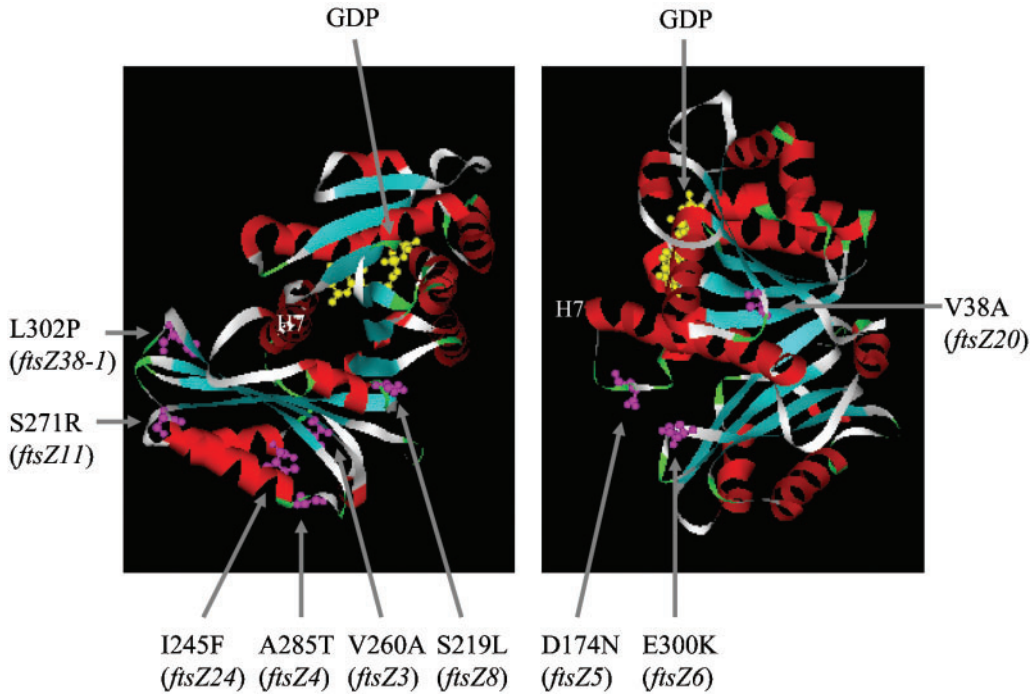

Fig. 5. Localization of the *ftsZ* mutations in the model of the structure of *B. subtilis* FtsZ. The residues altered by the mutations are shown in pink. The location of only the first mutation (*ftsZ38-1*; L302P) of the *ftsZ38* allele is indicated, as the second mutation *ftsZ38-2* (Q353R) lies in the extreme C-terminus, for which no structural data are available. The N-terminal domain contains a modelled molecule of GDP (yellow). Helix 7 (H7), which connects the N- and C-terminal domains of FtsZ, is indicated.

invaginated septa (Addinall & Lutkenhaus, 1996). The mutant turned out to have an insertion of six additional amino acids between amino acids 38 and 39 of FtsZ. Interestingly, the *ftsZ20* mutant strain, which exhibits a similar phenotype to the *ftsZ26* mutant (Figs 1 and 3), carries a single valine to alanine substitution at position 38. These data strongly support the notion that the shape of the FtsZ ring dictates the pattern of septal ingrowth (Addinall & Lutkenhaus, 1996), and it appears that residue V38 is directly involved in determining the direction of polymerization, and, when altered, leads to the formation of FtsZ spirals, and thus to twisted cells. The fact that several mutant proteins, and especially FtsZS271R (*ftsZ11*), formed FtsZ spirals, but no twisted cells were detected, suggests that the mutant FtsZ spirals seen by IFM differed in their ability to direct the shape of the invaginating septum. Alternatively, the shape of the FtsZ ring might not be enough to determine the shape of the invaginating septum.

Stricker & Erickson (2003) isolated *ftsZ* mutations in *E. coli* that formed extensive spirals, but were not capable of cell division. Production of the FtsZS271R (*ftsZ11*) mutant protein caused a similar phenotype, but here the mutant FtsZ is partially functional, as normal and filamentous cells were observed (Figs 1 and 3). It seems that long spirals extending over the nucleoid are formed in *B. subtilis* under various conditions, e.g. in a *noc* mutant strain, or in cells undergoing sporulation where formation of a spiral-like filament is an intermediate step of the switch from medial to polar FtsZ position (Ben-Yehuda & Losick, 2002; Wu & Errington, 2004).

Interestingly, a number of mutant proteins [FtsZV260A (*ftsZ3*), FtsZA285T (*ftsZ4*) and FtsZI245F (*ftsZ24*)] caused the formation of a significant amount of DNA-free minicells (Fig. 1, Table 2). The approximately normal cell length, and the ability to form discrete linear FtsZ bands similar to those of the wild-type (Figs 3), imply that the mutated FtsZs retained their normal assembly and constriction function. The formation of minicells suggests that these mutant proteins are less sensitive to the destabilizing action of MinC. The mutations probably do not abolish binding to MinC completely, as the amounts of minicells are not as high as in a *min* mutant strain (Marston *et al.*, 1998). Alternatively, the mutant proteins might form more stable polymers, and thereby be more resistant to the action of MinC. It is interesting that all three mutated residues are located quite close together on the FtsZ protein (Fig. 5). Bi & Lutkenhaus (1990) isolated SulA-resistant *ftsZ* mutants in *E. coli* that also formed increased levels of minicells, but the mutations lie at different sites compared with the above-mentioned *B. subtilis ftsZ* mutations.

The *ftsZ38* mutant (producing FtsZL302P-Q353R mutant

protein) differed from all of the others in being drastically affected in sporulation and activation of σ^F (Fig. 4), even though preliminary light microscopy experiments suggested that medial and asymmetric division are near normal. Previously, an *ftsA* mutant with aberrant asymmetric septa, but no defect in vegetative growth, has been described (Kemp *et al.*, 2002; Young, 1976), suggesting that FtsA protein has a distinct or additional role in asymmetric septation compared with vegetative division. The phenotype of the *ftsZ38* mutation suggests that FtsZ may also have a modified role in asymmetric septation, either directly or indirectly via FtsA. Alternatively, the FtsZL302P-Q353R mutant protein may be affected in binding, and thereby localizing the sporulation-specific division protein SpoIIE (Lucet *et al.*, 2000).

In conclusion, *B. subtilis* appears to be a good organism in which to create and study mutations in the essential *ftsZ* gene. The easy integration of the *ftsZ* alleles into the chromosome, and thus disruption of the wild-type copy of *ftsZ*, allows the viability and morphological phenotype of the mutants to be examined directly. Screening the mutant library for efficient sporulation (as an indication for changes in vegetative and/or asymmetric division) seemed to be quite sensitive, as we were able to isolate mutations with a range of mild phenotypes. Large-scale characterization of *ftsZ* mutants by this approach may help to shed light on the crucial questions of the role of FtsZ in assembly and constriction of the division machinery, and its coupling with cell growth, chromosome replication and segregation.

ACKNOWLEDGEMENTS

We thank David Brown for his help with the structural model of the *B. subtilis* FtsZ protein, Dirk-Jan Scheffers for helpful comments on the manuscript, and Richard Losick for strain FG356. This work was supported by grants from the Biotechnology and Biological Sciences Research Council (BBSRC) and the Medical Research Council (MRC).

REFERENCES

Addinall, S. G. & Lutkenhaus, J. (1996). FtsZ-spirals and -arcs determine the shape of the invaginating septa in some mutants of *Escherichia coli*. *Mol Microbiol* **22**, 231–237.

Anagnostopoulos, C. & Spizizen, C. (1961). Requirements for transformation in *Bacillus subtilis*. *J Bacteriol* **81**, 741–746.

Barak, I. & Youngman, P. (1996). *SpoIIE* mutants of *Bacillus subtilis* comprise two distinct phenotypic classes consistent with a dual functional role for the SpoIIE protein. *J Bacteriol* **178**, 4984–4989.

Beall, B. & Lutkenhaus, J. (1992). Impaired cell division and sporulation of a *Bacillus subtilis* strain with the *ftsA* gene deleted. *J Bacteriol* **174**, 2398–2403.

Beall, B., Lowe, M. & Lutkenhaus, J. (1988). Cloning and characterization of *Bacillus subtilis* homologs of *Escherichia coli* cell division genes *ftsZ* and *ftsA*. *J Bacteriol* **170**, 4855–4864.

Ben-Yehuda, S. & Losick, R. (2002). Asymmetric cell division in *B. subtilis* involves a spiral-like intermediate of the cytokinetic protein FtsZ. *Cell* **109**, 257–266.

Bi, E. & Lutkenhaus, J. (1990). Analysis of *ftsZ* mutations that confer resistance to the cell division inhibitor SulA (SfiA). *J Bacteriol* **172**, 5602–5609.

Bi, E. & Lutkenhaus, J. (1992). Isolation and characterization of *ftsZ* alleles that affect septal morphology. *J Bacteriol* **174**, 5414–5423.

Bramhill, D. & Thompson, C. M. (1994). GTP-dependent polymerization of *Escherichia coli* FtsZ protein to form tubules. *Proc Natl Acad Sci U S A* **91**, 5813–5817.

Daniel, R. A. & Errington, J. (2000). Intrinsic instability of the essential cell division protein FtsL of *Bacillus subtilis* and a role for DivIB protein in FtsL turnover. *Mol Microbiol* **36**, 278–289.

Daniel, R. A., Harry, E. J. & Errington, J. (2000). Role of penicillin-binding protein PBP 2B in assembly and functioning of the division machinery of *Bacillus subtilis*. *Mol Microbiol* **35**, 299–311.

Erickson, H. P., Taylor, D. W., Taylor, K. A. & Bramhill, D. (1996). Bacterial cell division protein FtsZ assembles into protofilament sheets and minirings, structural homologs of tubulin polymers. *Proc Natl Acad Sci U S A* **93**, 519–523.

Errington, J. (1984). Efficient *Bacillus subtilis* cloning system using bacteriophage vector ϕ105J9. *J Gen Microbiol* **130**, 2615–2628.

Errington, J. (2003). Regulation of endospore formation in *Bacillus subtilis*. *Nat Rev Microbiol* **1**, 117–126.

Errington, J. & Mandelstam, J. (1986). Use of a *lacZ* gene fusion to determine the dependence pattern of sporulation operon *spoIIA* in *spo* mutants of *Bacillus subtilis*. *J Gen Microbiol* **132**, 2967–2976.

Errington, J., Daniel, R. A. & Scheffers, D. J. (2003). Cytokinesis in bacteria. *Microbiol Mol Biol Rev* **67**, 52–65.

Feucht, A., Magnin, T., Yudkin, M. D. & Errington, J. (1996). Bifunctional protein required for asymmetric cell division and cell-specific transcription in *Bacillus subtilis*. *Genes Dev* **10**, 794–803.

Feucht, A., Daniel, R. A. & Errington, J. (1999). Characterization of a morphological checkpoint coupling cell-specific transcription to septation in *Bacillus subtilis*. *Mol Microbiol* **33**, 1015–1026.

Feucht, A., Lucet, I., Yudkin, M. D. & Errington, J. (2001). Cytological and biochemical characterization of the FtsA cell division protein of *Bacillus subtilis*. *Mol Microbiol* **40**, 115–125.

Feucht, A., Abbotts, L. & Errington, J. (2002). The cell differentiation protein SpoIIE contains a regulatory site that controls its phosphatase activity in response to asymmetric septation. *Mol Microbiol* **45**, 1119–1130.

Gueiros-Filho, F. J. & Losick, R. (2002). A widely conserved bacterial cell division protein that promotes assembly of the tubulin-like protein FtsZ. *Genes Dev* **16**, 2544–2556.

Haeusser, D. P., Schwartz, R. L., Smith, A. M., Oates, M. E. & Levin, P. A. (2004). EzrA prevents aberrant cell division by modulating assembly of the cytoskeletal protein FtsZ. *Mol Microbiol* **52**, 801–814.

Jenkinson, H. F. (1983). Altered arrangement of proteins in the spore coat of a germination mutant of *Bacillus subtilis*. *J Gen Microbiol* **129**, 1945–1958.

Katis, V. L., Wake, R. G. & Harry, E. J. (2000). Septal localization of the membrane-bound division proteins of *Bacillus subtilis* DivIB and DivIC is codependent only at high temperatures and requires FtsZ. *J Bacteriol* **182**, 3607–3611.

Kemp, J. T., Driks, A. & Losick, R. (2002). FtsA mutants of *Bacillus subtilis* impaired in sporulation. *J Bacteriol* **184**, 3856–3863.

Khvorova, A., Zhang, L., Higgins, M. L. & Piggot, P. J. (1998). The *spoIIE* locus is involved in the Spo0A-dependent switch in the location of FtsZ rings in *Bacillus subtilis*. *J Bacteriol* **180**, 1256–1260.

King, N., Dreesen, O., Stragier, P., Pogliano, K. & Losick, R. (1999). Septation, dephosphorylation, and the activation of σ^F during sporulation in *Bacillus subtilis*. *Genes Dev* **13**, 1156–1167.

Levin, P. A., Shim, J. J. & Grossman, A. D. (1998). Effect of *minCD* on FtsZ ring position and polar septation in *Bacillus subtilis*. *J Bacteriol* **180**, 6048–6051.

Lewis, P. J. & Errington, J. (1996). Use of green fluorescent protein for detection of cell-specific gene expression and subcellular protein localization during sporulation in *Bacillus subtilis*. *Microbiology* **142**, 733–740.

Low, H. H., Moncrieffe, M. C. & Lowe, J. (2004). The crystal structure of ZapA and its modulation of FtsZ polymerization. *J Mol Biol* **341**, 839–852.

Lowe, J. & Amos, L. A. (1998). Crystal structure of the bacterial cell-division protein FtsZ. *Nature* **391**, 203–206.

Lowe, J. & Amos, L. A. (1999). Tubulin-like protofilaments in Ca^{2+}-induced FtsZ sheets. *EMBO J* **18**, 2364–2371.

Lucet, I., Feucht, A., Yudkin, M. D. & Errington, J. (2000). Direct interaction between the cell division protein FtsZ and the cell differentiation protein SpoIIE. *EMBO J* **19**, 1467–1475.

Ma, X. & Margolin, W. (1999). Genetic and functional analyses of the conserved C-terminal core domain of *Escherichia coli* FtsZ. *J Bacteriol* **181**, 7531–7544.

Marston, A. L. & Errington, J. (1999). Selection of the midcell division site in *Bacillus subtilis* through MinD-dependent polar localization and activation of MinC. *Mol Microbiol* **33**, 84–96.

Marston, A. L., Thomaides, H. B., Edwards, D. H., Sharpe, M. E. & Errington, J. (1998). Polar localization of the MinD protein of *Bacillus subtilis* and its role in selection of the mid-cell division site. *Genes Dev* **12**, 3419–3430.

Meissner, P. S., Sisk, W. P. & Berman, M. L. (1987). Bacteriophage λ cloning system for the construction of directional cDNA libraries. *Proc Natl Acad Sci U S A* **84**, 4171–4175.

Mosyak, L., Zhang, Y., Glasfeld, E., Haney, S., Stahl, M., Seehra, J. & Somers, W. S. (2000). The bacterial cell-division protein ZipA and its interaction with an FtsZ fragment revealed by X-ray crystallography. *EMBO J* **19**, 3179–3191.

Mukherjee, A. & Lutkenhaus, J. (1994). Guanine nucleotide-dependent assembly of FtsZ into filaments. *J Bacteriol* **176**, 2754–2758.

Mukherjee, A. & Lutkenhaus, J. (1998). Dynamic assembly of FtsZ regulated by GTP hydrolysis. *EMBO J* **17**, 462–469.

Nogales, E., Wolf, S. G. & Downing, K. H. (1998). Structure of the $\alpha\beta$ tubulin dimer by electron crystallography. *Nature* **391**, 199–203.

Palacios, P., Vicente, M. & Sanchez, M. (1996). Dependency of *Escherichia coli* cell-division size, and independency of nucleoid segregation on the mode and level of *ftsZ* expression. *Mol Microbiol* **20**, 1093–1098.

Partridge, S. R. & Errington, J. (1993). The importance of morphological events and intercellular interactions in the regulation of prespore-specific gene expression during sporulation in *Bacillus subtilis*. *Mol Microbiol* **8**, 945–955.

Pogliano, K., Harry, E. & Losick, R. (1995). Visualization of the subcellular location of sporulation proteins in *Bacillus subtilis* using immunofluorescence microscopy. *Mol Microbiol* **18**, 459–470.

Resnekov, O., Alper, S. & Losick, R. (1996). Subcellular localization of proteins governing the proteolytic activation of a developmental transcription factor in *Bacillus subtilis*. *Genes Cells* **1**, 529–542.

Romberg, L. & Levin, P. A. (2003). Assembly dynamics of the bacterial cell division protein FtsZ: poised at the edge of stability. *Annu Rev Microbiol* **57**, 125–154.

Sambrook, J., Fritsch, E. F. & Maniatis, T. (1989). *Molecular Cloning: a Laboratory Manual*, 2nd edn. Cold Spring Harbor, NY: Cold Spring Harbor Laboratory.

Scheffers, D. J., de Wit, J. G., den Blaauwen, T. & Driessen, A. J. (2002). GTP hydrolysis of cell division protein FtsZ: evidence that the active site is formed by the association of monomers. *Biochemistry* **41**, 521–529.

Sharpe, M. E., Hauser, P. M., Sharpe, R. G. & Errington, J. (1998). *Bacillus subtilis* cell cycle as studied by fluorescence microscopy: constancy of cell length at initiation of DNA replication and evidence for active nucleoid partitioning. *J Bacteriol* **180**, 547–555.

Sievers, J., Raether, B., Perego, M. & Errington, J. (2002). Characterization of the *parB*-like *yyaA* gene of *Bacillus subtilis*. *J Bacteriol* **184**, 1102–1111.

Sterlini, J. M. & Mandelstam, J. (1969). Commitment to sporulation in *Bacillus subtilis* and its relationship to development of actinomycin resistance. *Biochem J* **113**, 29–37.

Stevens, C. M., Daniel, R., Illing, N. & Errington, J. (1992). Characterization of a sporulation gene, *spoIVA*, involved in spore coat morphogenesis in *Bacillus subtilis*. *J Bacteriol* **174**, 586–594.

Stricker, J. & Erickson, H. P. (2003). *In vivo* characterization of *Escherichia coli ftsZ* mutants: effects on Z-ring structure and function. *J Bacteriol* **185**, 4796–4805.

Thomaides, H. B., Freeman, M., El Karoui, M. & Errington, J. (2001). Division site selection protein DivIVA of *Bacillus subtilis* has a second distinct function in chromosome segregation during sporulation. *Genes Dev* **15**, 1662–1673.

Vaughan, S., Wickstead, B., Gull, K. & Addinall, S. G. (2004). Molecular evolution of FtsZ protein sequences encoded within the genomes of archaea, bacteria, and eukaryota. *J Mol Evol* **58**, 19–29.

Wang, X., Huang, J., Mukherjee, A., Cao, C. & Lutkenhaus, J. (1997). Analysis of the interaction of FtsZ with itself, GTP, and FtsA. *J Bacteriol* **179**, 5551–5559.

Ward, J. E., Jr & Lutkenhaus, J. (1985). Overproduction of FtsZ induces minicell formation in *E. coli*. *Cell* **42**, 941–949.

Weart, R. B. & Levin, P. A. (2003). Growth rate-dependent regulation of medial FtsZ ring formation. *J Bacteriol* **185**, 2826–2834.

Wu, L. J. & Errington, J. (2004). Coordination of cell division and chromosome segregation by a nucleoid occlusion protein in *Bacillus subtilis*. *Cell* **117**, 915–925.

Young, M. (1976). Use of temperature-sensitive mutants to study gene expression during sporulation in *Bacillus subtilis*. *J Bacteriol* **126**, 928–936.

Yu, X. C. & Margolin, W. (1997). Ca^{2+}-mediated GTP-dependent dynamic assembly of bacterial cell division protein FtsZ into asters and polymer networks *in vitro*. *EMBO J* **16**, 5455–5463.